Low-order acoustic prediction tool for estimating noise emissions from distributed propeller configurations

do Nascimento Monteiro, F.; Ragni, D.; Avallone, F.; Sinnige, T.

Low-Order Acoustic Prediction Tool for Estimating Noise Emissions From Distributed Propeller Configurations

Fernanda do N. Monteiro[*,a], Daniele Ragni [†,a], Francesco Avallone [‡b], and Tomas Sinnige [§,a]

[a]*Delft University of Technology, Delft 2629HS, The Netherlands*
[b]*Polytechnic of Turin, Turin, 10129, Italy*

A low-order numerical tool for estimating noise emissions from distributed propeller configurations is presented. The paper describes the tool's computational framework, which uses Hanson's near-field theory to calculate the thickness and loading noise components. The formulation assumes steady blade loading, but an unsteady case can be handled numerically by redefining the pressure distribution over the blade at each new time step. Two representative cases are analyzed to validate the tool: an isolated propeller operating in uniform flow and an array of three propellers in a side-by-side configuration under aerodynamic interference caused by adjacent propellers. The results obtained from the low-fidelity tool are compared to high-fidelity data to evaluate the accuracy and differences in predicting the noise of a distributed propeller system. The low-fidelity tool provides accurate results for both cases, with less than a 1.5 dB difference up to the fifth blade-passage frequency (BPF) when comparing tonal noise predictions at an observer located 10 diameters away and at the propeller plane. When analyzing the source directivity at the first BPF, there is a difference of approximately 0.5 dB at the propeller plane. However, this difference increases to 6 dB as the observer moves toward the inflow direction. This difference is due to the dominance of broadband noise near the propeller axis. The paper concludes with a noise analysis of the distributed propeller system, examining the relative importance of aerodynamic interference in the noise emitted by a propeller. In this case, the unsteady blade loading generated a tonal component of 40 dB at the first BPF in the propeller axis, while it had an insignificant effect at the rotor plane.

I. Nomenclature

D	=	propeller diameter
h	=	blade thickness distribution
M_r	=	local blade element Mach number
$\hat{\mathbf{n}}$	=	unit vector normal to the helical surface
p'	=	acoustic pressure
$\mathbf{R}$	=	distance from source point to observer
$\mathbf{r}$	=	distance from origin to observer
$\mathbf{r}_o$	=	distance from origin to source point
r_o	=	radial distance to the propeller shaft
r_{hub}	=	blade hub radius
r_{tip}	=	blade tip radius
t	=	reception time
U	=	local helical speed of the source
γ	=	distance backward in the helical surface
Δp	=	difference between upper and lower surface pressure on the blade
ξ	=	normal coordinate to the helical surface
ρ	=	ambient density

---

[*]PhD candidate, Wind Energy Section, Fac. of Aerospace Eng., F.doNascimentoMonteiro@tudelft.nl.

[†]Associate Professor, Wind Energy Section, Fac. of Aerospace Eng., D.Ragni@tudelft.nl, AIAA Member.

[‡]Assistant Professor, Department of Mechanical and Aerospace Engineering, Polytechnic of Turin, Francesco.Avallone@polito.it, AIAA Member

[§]Assistant Professor, Flight Performance and Propulsion Section, Fac. of Aerospace Eng., AIAA Member

τ =   emission time

II. Introduction

THE Flightpath 2050 report [1], developed by the Advisory Council Research and Innovation in Europe (ACARE), sets ambitious goals for aircraft in 2050. These goals include reducing CO_2 emissions by 75%, NO_x emissions by 90%, and perceived noise emissions by 65% compared to 2000 levels. However, standard technologies in current aircraft are reaching their development limits, making incremental enhancements insufficient to meet these demands. Innovative and breakthrough designs with superior propulsive efficiency will be necessary in the near future to fulfill these requirements. One suggested design is the distributed electric propulsion (DEP) configuration, which proposes an optimized arrangement of multiple electric motor-driven propulsors along the airframe to enhance aerodynamic, propulsive, and structural efficiency [2–5].

One of the many reasons to invest in DP systems is the possibility of distributing the overall required thrust of the aircraft to its multiple propellers. Consequently, the distribution of thrust over the airframe enables opportunities for smart propulsion integration with beneficial interaction effects on the airframe performance. In addition, DEP architectures composed of propellers can reduce noise through synchrophasing [6–8], which involves synchronizing the relative blade phase angle to obtain destructive interferences of multiple propeller sound fields at a specific location. Although this technique has been studied for decades to reduce cabin noise in propeller-driven airplanes [9–13], most studies on DEP configurations have only evaluated the acoustic interference effects on noise. However, in highly integrated architectures, the aerodynamic interaction between components may modify the acoustic field by changing the noise source strength [14–17].

Bernardini et al. [14, 15] conducted a numerical study on the acoustic interaction effects of arrays with two and three rotors. They found that aerodynamic interference increased the noise emitted in the forward direction, broadened the high-noise region (near the propeller plane), and increased the noise peak compared to simulations that only assumed acoustic interference. de Vries et al. [18] showed in their experiments with an array of three propellers that the resulting acoustic waveform can be predicted by superimposing the acoustic waveform of individual propellers, but only when the propellers are installed sufficiently far from each other (equal to one propeller radius). However, this approximation cannot be used when the blade tip distance between adjacent propellers is lower than 4% of the propeller radius. In this condition, the aerodynamic interaction between the blades of adjacent propellers adds a significant noise contribution. On the other side, Poggi et al. [17] demonstrated in their numerical investigation that the decrease of the tip clearance between propellers favorably affects the radiated noise, reducing both the average and the maximum overall sound pressure level (OASPL), with negligible directivity changes.

The different results in these studies emphasize the need to understand better the impact of aerodynamic interference on the acoustic footprint of distributed propeller (DP) systems. Therefore, this paper presents a low-order numerical acoustic tool capable of investigating the impact of the aerodynamic interference on the acoustics of multiple propellers. It is designed to be computationally efficient and provide quick results. The tool is based on a simplified time-domain model of the tonal acoustic sources presented by Hanson [19]. It is intended to be used early in the design process to evaluate the acoustic performance of a new configuration and guide the design process. While the low-order numerical tool may not produce results as precise as high-fidelity simulations in areas where broadband noise dominates (such as near the propeller axis), it still provides a valuable estimation of noise emissions and can be utilized for comparing the acoustic efficiency of various configurations. Even so, this limitation can be diminished by adding a broadband model to the tool.

The remainder of this paper is structured as follows. First, Sec. III provides a brief overview of the tool, with Sec. III.A supplying the theoretical formulations, and Sec. III.B describing the computational framework. Section IV presents two representative cases used to validate the tool: the first case calculates the noise emitted by an isolated propeller, and the second one calculates the noise emitted by an array of three propellers. An example of how the low-order numerical tool for estimating noise emissions from distributed propeller configurations can be applied is presented in Sec. V. Finally, Sec. VI summarizes the main outcomes, the limits and capabilities of the tool, and future work.

III. Methodology

A. Theoretical Formulation

Hanson's 1976 near-field theory [19] describes the tonal noise generated by propellers operating at supersonic or high subsonic tip speeds. This theory is based on the Ffowcs-Williams and Hawkings equation [20]. As the focus is on propeller application, the quadrupole term that depends on Lighthill's stress tensor is neglected. Thus, only the monopole and dipole terms, which are responsible for the thickness and loading tonal noise components, are considered in Hanson's near-field theory.

The theory presented in this document uses a helical coordinate system and a noise source description in the stationary reference frame, instead of the blade-fixed coordinate system. This approach avoids mathematical singularities that arise when the source moves toward the observer's direction at sonic speed [21–23]. However, the time-domain method requires computing acoustic planforms at each time step and integrating over them to calculate the tonal noise components. The acoustic planform method poses a challenge due to the variation of its area over time. When the blade is approaching the observer at maximum speed, it has a maximum chordwise length, and its area splits into two distinct regions when the Mach number towards the observer is greater than one. However, the acoustic planform highlights the non-compactness of the noise source at high speeds.
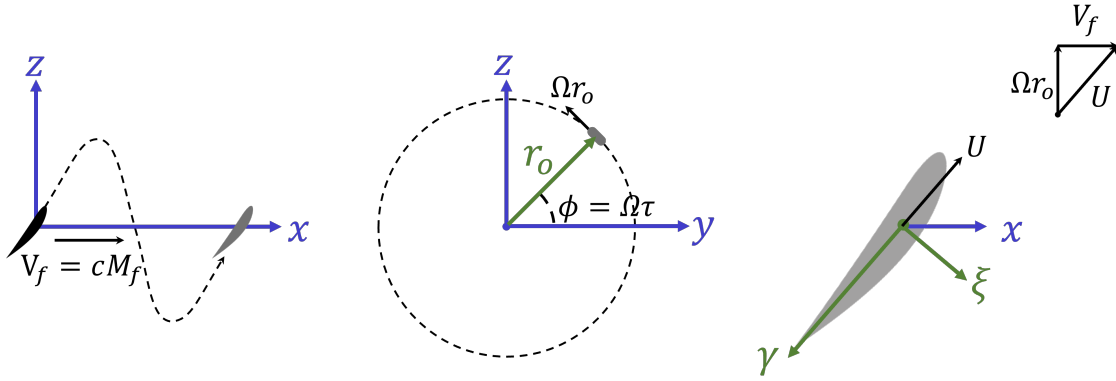

Fig. 1 Helical and Cartesian coordinate systems (adapted from Ref. [19]).

During forward flight, the blade moves along a helical surface defined by its angular velocity $\mathbf{\Omega}$ and the flight speed $\mathbf{V}_f$. Hence, the position of its elements is expressed in the helical coordinate system as (r_o, γ, ξ), where r_o is the radial distance to the propeller shaft, γ is the distance backward in the helical surface, and ξ is normal to the helical surface (figure 1). The parameter $\mathbf{U}$ represents the blade element's local velocity and points in the negative direction of the γ-axis. At time $t = 0$, the blade pitch change axis (PCA) is aligned with the y-axis. The coordinate ξ is expressed in terms of the thickness distribution function $h(\gamma, r_o)$.

As mentioned, the emission surface is created by projecting the upper and lower surfaces of the blade onto the chord line of each radial section. Therefore, it is assumed that the volume displacement and the force imposed by the blade on the fluid act on this fixed surface within the fluid. As a result, the distance between the source and observer $\mathbf{R}$ is independent of time, and the source function is formulated to activate at the helical surface in a way that corresponds precisely to the movement of the blade through the use of a Green's function.

The formulas for computing the tonal noise components of a rotating blade are shown below. The derivation and alternative forms are presented in Ref. [19]. The acoustic pressure related to blade thickness, p'_{TH}, is given by Eq. 1. The pressure related to blade loading is divided into its near- and far-field components: p'_{LN} and p'_{LF}, respectively, given by equations 2 and 3.

$$p'_{\mathrm{TH}}(\mathbf{r}, t) = \int_{r_{\mathrm{hub}}}^{r_{\mathrm{tip}}} \int_{\gamma_{\mathrm{LE}}}^{\gamma_{TE}} \left[\left(\frac{\rho U^2}{4\pi R} \right) \frac{\partial^2}{\partial \gamma^2} h(\gamma, r_o) \right]_{\mathrm{ret}} \mathrm{d}\gamma \, \mathrm{d}r_o \tag{1}$$

$$p'_{\mathrm{LN}}(\mathbf{r}, t) = \int_{r_{\mathrm{hub}}}^{r_{\mathrm{tip}}} \int_{\gamma_{\mathrm{LE}}}^{\gamma_{TE}} \left[\left(\frac{\mathbf{R} \cdot \hat{\mathbf{n}}}{4\pi R^3} \right) \Delta p(\gamma, r_o) \right]_{\mathrm{ret}} \mathrm{d}\gamma \, \mathrm{d}r_o \tag{2}$$

3

$$p'_{\text{LF}}\left(\mathbf{r}, t\right) = \frac{\partial}{\partial t} \int_{r_{\text{hub}}}^{r_{\text{tip}}} \int_{\gamma_{\text{LE}}}^{\gamma_{TE}} \left[\left(\frac{M_r \mathbf{R} \cdot \hat{\mathbf{n}}}{4\pi R^2} \right) \frac{\partial}{\partial \gamma} \Delta p\left(\gamma, r_o\right) \right]_{\text{ret}} d\gamma \, dr_o \qquad (3)$$

The parameter $\mathbf{r}$ is the observer position, t is the reception time, ρ is the density of the undisturbed medium, U is the source local speed, R is the distance from the source to the observer, $\hat{\mathbf{n}}$ is the unit vector normal to the helical surface, and Δp is the pressure distribution over the blade. The integration limits for all formulae are defined by the radial coordinates of the hub, r_{hub}, and the tip, r_{tip}, and the helical coordinates of the leading edge, γ_{LE}, and the trailing edge, γ_{TE}, at their retarded time. These limits delineate the acoustic planform, which is the surface constructed by assembling sources loci at their emission time t_o.

The equations predict the thickness and loading noise of one blade. In order to calculate the propeller noise, the acoustic pressure of each blade is superimposed while taking their positions into account. Likewise, for a distributed propeller system, the noise at the observer's location is computed by superposing the acoustic pressure of all propellers and considering their positions within the system.

B. Computational Framework

Several factors need to be considered to predict the noise from a distributed propeller system. In addition to basic inputs such as operating conditions and aerodynamic data, the system and observer must be positioned relative to each other, as well as to the propellers' arrangement within the system. Then, parameters of interest must be computed at the source time to obtain the acoustic planform at the reception time. The thickness and loading noise components are then calculated, so the acoustic waveforms of each blade can be superposed to obtain the noise at the observer's location. Figure 2 illustrates the main steps of this computational framework.
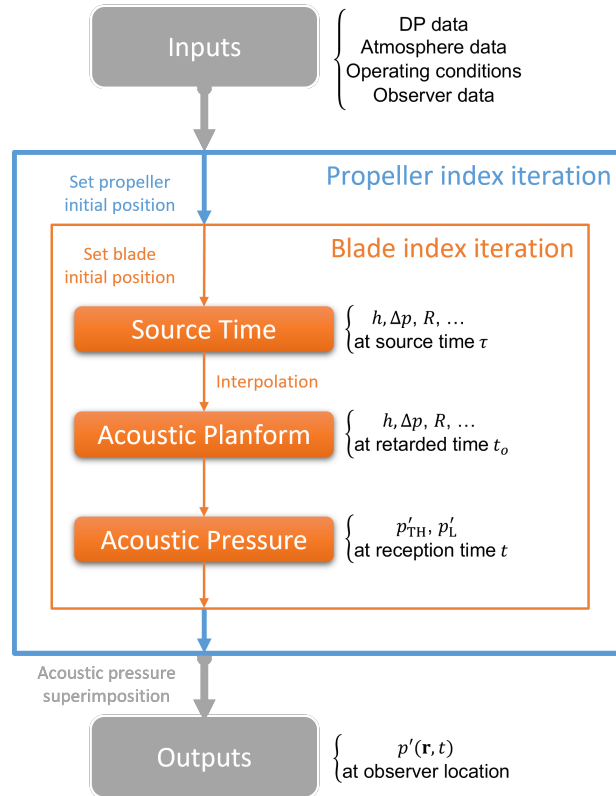

Fig. 2   Diagram of the code architecture.

Basic input data is required to compute the noise of a DP system as received by an observer. These include atmosphere properties data, DP geometrical and coordinate data, operation conditions, propeller and blade geometrical data, and pressure distribution over the blade surface. When aerodynamic interaction is considered, the pressure distribution data should be provided in the time domain, so the loading over the blade can be updated at each new time

4

point calculated. Likewise, if the observer is in motion, it is necessary to include information about its movement to determine its location at each time step. Additionally, the user must also define other parameters, such as the number of temporal steps per period and the number of points on the blade mesh grid in the radial and chordwise directions.

Once the inputs are loaded, the reception time is evaluated for every discrete surface element at each defined source time. The signal is stored at each time step, containing all the parameters necessary to compute the integrand of the above equations. Next, a constant time step sequence is defined for the observer, and the acoustic planform at each selected reception time is obtained by interpolating the values of the blade element positions stored in the previous step. Similarly, the values needed to compute Eqs. 1, 2, and 3 are obtained through interpolation.

In order to calculate the acoustic pressure, a double integral is performed over the chordwise and radial directions of each blade. This yields the thickness and loading noise components of each blade. Once the pressure is computed, the acoustic waveforms are superimposed to obtain the total noise at the observer's location. Basically, the process involves adding up the contributions of each blade to determine the overall noise emitted by the distributed propeller system.

As previously noted, Hanson's near-field theory avoids the mathematical singularity that arises when elements of the blade surface move toward the observer at sonic speed. However, the current code does not handle sonic cases. The problem arises when the component of the source Mach number in the observer direction exceeds 1, leading to increasing distortions on the acoustic planform. When parts of the surface exceed the sonic speed, the acoustic planform of one blade splits into two sections because some elements emit signals at different instants, even though they arrive simultaneously at the observer. This means that multiple roots occur for a single observer time. To account for this scenario, the interpolation used in the computation to obtain the retarded time needs to be capable of obtaining both values, which it is currently incapable of doing.

As stated, the overall thrust required by an aircraft with a DP system is distributed between multiple propellers. Consequently, each propulsion unit can deliver less thrust and be designed with a smaller diameter. This implies fewer patches of the blade surface reach sonic speeds, avoiding performance losses and additional noise due to transonic effects. As a result, a propeller in a DP system typically operates in the subsonic regime. Therefore, the low-order numerical tool presented for estimating noise emissions from distributed propeller configurations is suitable for most DP systems currently under investigation.

IV. Tool Validation

The method presented in Sec. III is validated through two representative cases. The first one involves an isolated propeller operating in uniform flow. The second case involves an array of three propellers in a side-by-side configuration under aerodynamic interference caused by adjacent blades. The results from the low-fidelity tool are compared to high-fidelity data to determine its potential for accurately predicting the noise of a DP system. The acoustic data for both cases was obtained from high-fidelity simulations using the SIMULIA PowerFLOW CFD solver based on the Lattice Boltzmann Very Large Eddy Simulation (LB/VLES) method, coupled with a Ffwocs-Williams and Hawkings (FW-H) acoustic analogy [24, 25].

First, the isolated propeller case is presented. The objective is to evaluate the tool's ability to predict the noise emitted by a simple system composed of one propeller in a uniform flow field. Therefore, the primary purpose is to assess the tool's potential for predicting propeller noise. Then, the code is tested to predict the noise emitted by an array of propellers operating with a tip clearance of 4% of the propeller radius and a relative blade phase angle of 0 degree. At this distance, aerodynamic interference between adjacent blades impact the pressure distribution near the blade tip, affecting the source strength. By analyzing the results of both cases, it is possible to evaluate the tool's accuracy in predicting the noise generated by a distributed propeller system.

A. Case 1: Isolated Propeller

In order to validate the tool, it is necessary to investigate its effectiveness in predicting the noise of a simple system consisting of one propeller without any aerodynamic interference (an isolated propeller). This requires accurate and validated aerodynamic and acoustic data, as well as detailed geometry and operational condition parameters. For this purpose, the study conducted by Fuerkaiti et al. [24] was chosen as a reference.

In their analysis, the authors presented a framework for predicting the noise footprint of propeller-driven aircraft to investigate the acoustic impact of design and operating parameters. Their validation case consisted of an isolated propeller in cruise conditions, and the results were compared against high-fidelity data. The low-fidelity approach used in their study is based on the frequency-domain acoustic theory also derived by Hanson [26].

Table 1 lists the geometric parameters and operating conditions of the propeller. The radial distributions of the chord

and twist are shown in Fig. 3b. The propeller operates at a rotational speed of 1900 rpm and a flight Mach number of $M_f = 0.2$ while cruising at a 2 km altitude. This results in an advance ratio of $J = 0.84$. The seven-bladed propeller has a diameter of $D = 2.5$ m and a hub-to-tip ratio of 0.1064. The observer is located in the propeller disk plane, defined in the Cartesian coordinates by $(0, 0, -10D)$.

Table 1   Parameters for the isolated propeller case

Parameter	Value	Unit
Flight altitude - h	2000	m
Flight Mach number - M_f	0.2	-
Propeller diameter - D	2.5	m
Hub-to-tip ratio - r_{hub}/r_{tip}	0.1064	-
Number of blades - N_B	7	-
Advance ratio - J	0.84	-

(a)   **(b)**
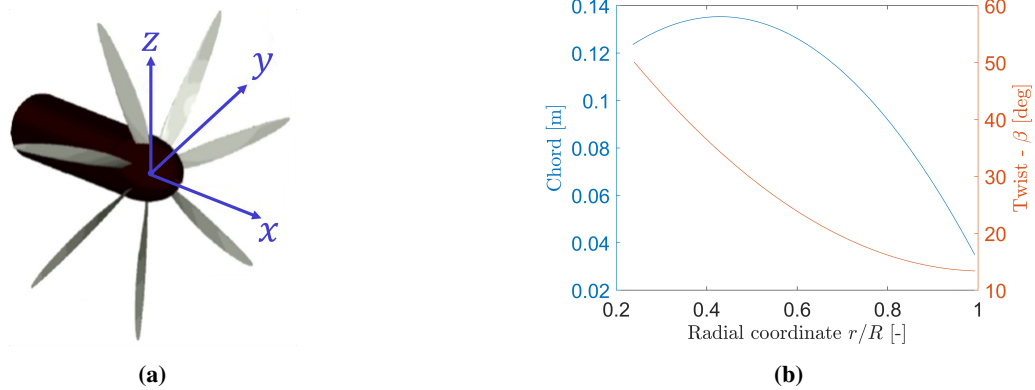
Fig. 3   Propeller geometry and the Cartesian reference frame (a) and blade chord and twist radial distributions (b) (adapted from Ref. [24]).

A Blade Element Momentum Theory (BEMT) was used to compute the aerodynamic data for the low-fidelity tool in the isolated propeller case. This allowed for testing the code's behavior when using low-fidelity aerodynamic loads. Also, the same data was used in the frequency-domain approach presented by Fuerkaiti et al. [24]. The authors showed that the aerodynamic data provided by the BEMT model agreed favorably with the high-fidelity simulation results, with a slight underprediction near the hub and tip and an overprediction in the rest of the blade. As mentioned earlier, using identical input enabled a well-founded comparison between the time- and frequency-domain models.

Three studies were conducted to assess the accuracy of the code in predicting the noise generated by an isolated propeller. The first study compared the predicted tonal contribution at the observer location to the results of high-fidelity simulations and frequency-domain analysis. Next, the impact of the number of time steps per period on the results was investigated. Finally, the third study investigated the source directivity results at the first blade passage frequency (BPF).

The computation used a blade mesh grid consisting of 51 points in the chordwise direction and 99 points in the radial direction, providing sufficient detail for the analysis. For time discretization, an initial estimate of 400 steps per period was used.

Figure 4 compares the tonal contribution computed by the low-fidelity tool (indicated as TD) against the results obtained from high-fidelity simulations (indicated as HF) and frequency-domain formulations (indicated as FD). The time-domain prediction shows excellent agreement with the high-fidelity data, as shown in Fig. 4a. Figure 4 displays the sound pressure level difference between the high-fidelity result and both low-fidelity data. For frequencies below the sixth BPF, the time-domain prediction has less than a 1.53 dB difference compared to the high-fidelity values.
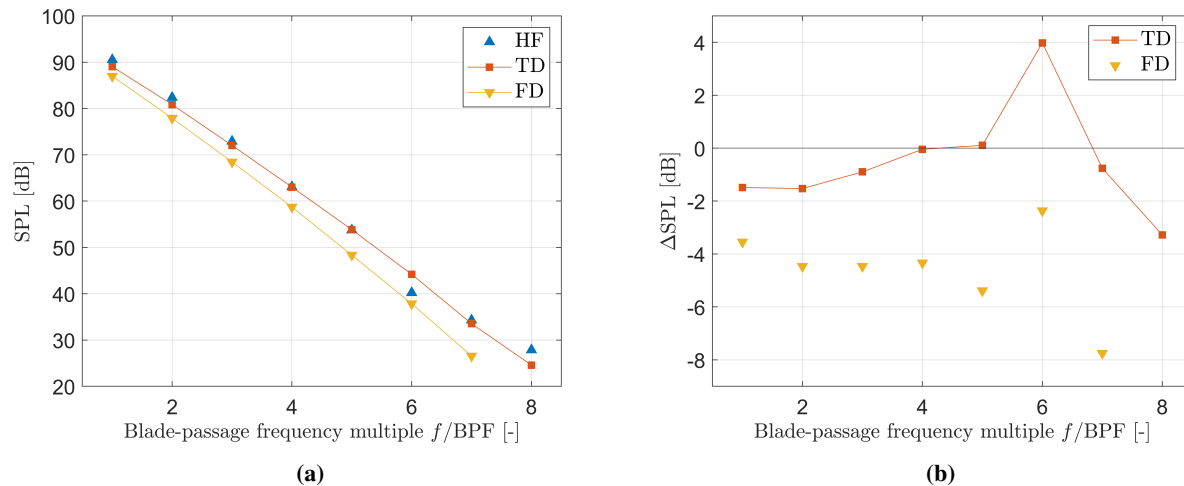
(a)   **(b)**

Fig. 4   Tonal noise prediction: (a) comparison between predictions, and (b) differences with respect to high-fidelity data.

In order to achieve accurate predictions, the number of time steps per period is an essential factor to consider, as the code relies on a time-domain approach. Hence, the same case was analyzed using different time samplings per period, as shown in Fig. 5. Computed values indicated that increasing from 200 to 400 time steps did not significantly change the first BPF. However, there was a slight improvement between the second and fifth harmonics. Further increasing from 400 to 600 time steps did not significantly change the results. Therefore, the subsequent analyses were conducted using 400 time samples per period.
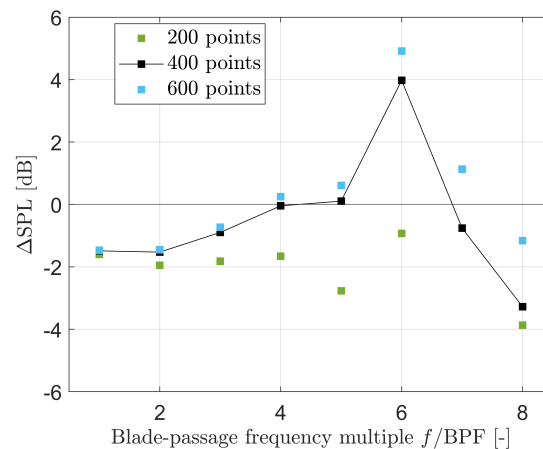

Fig. 5   Impact of the number of time steps per period on the results.

The analysis of the source directivity at the first BPF concludes the validation of the low-order numerical tool applied to the isolated case. Fig. 6 shows data points at a radial distance of 10 diameters from the propeller center. For all planes, the time-domain tool captured the trend of high-fidelity predictions well. The outputs agree satisfactorily between 210° and 330°, with discrepancies of less than 6 and 4 dB at the xy- and xz-planes, respectively. Unsurprisingly, the code computes zero levels near the propeller axis, seeing that the broadband noise component dominates at those locations. The closest agreements are at the yz-plane, with a difference of less than 1 dB. Overall, the analysis of source directivity demonstrated the effectiveness and limitations of the low-order numerical tool in capturing the trend of high-fidelity noise predictions of an isolated propeller.
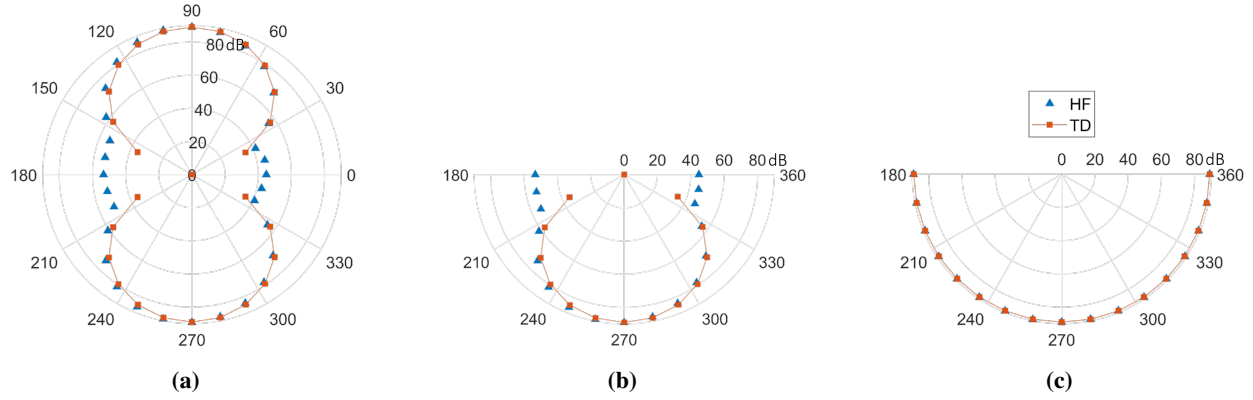
7

(a)   **(b)**   **(c)**

Fig. 6   **Source directivity at the first BPF at (a)** xy**-plane, (b)** xz**-plane and (c)** yz**-plane.**

B. Case 2: Array of Propellers

After validating the tool for a single propeller under steady blade loading, it is essential to analyze its capacity to predict the noise generated by multiple propellers under aerodynamic interaction. The complex flow behavior in these configurations can significantly affect the noise emitted by the system. Therefore, accurate aerodynamic data are essential to compute a more precise acoustic prediction. To this end, the aerodynamic input used for the tool should come from high-fidelity simulations, as they provide more detailed information on the flow over the blade surface. Therefore, the numerical study conducted by **?** [**?**] was chosen as a reference.

In the analysis, three identical propellers are arranged side-by-side along the y-axis (Fig. 7a). Table 2 lists the geometric parameters and operating conditions. The tip clearance between the propellers is 2% of their diameters, and the relative blade phase angle is $\Delta\phi = 0$ °. The propellers have six blades, a diameter of $D = 0.2032$ m, and a hub-to-tip ratio of $r_{\text{hub}}/r_{\text{tip}} = 0.1095$. Details about the blade chord and pitch radial distributions are given in Fig. 7b, and additional information about the propellers is available in the previous study [27].
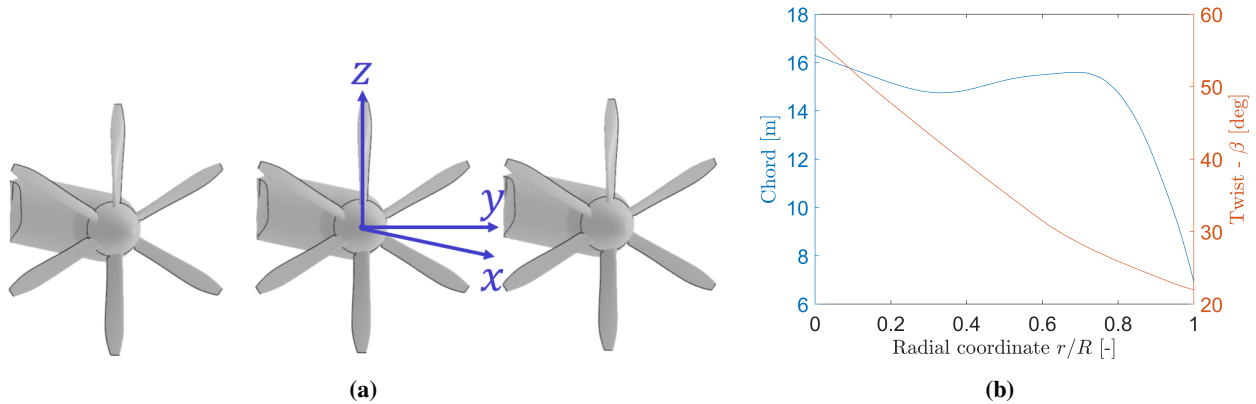

(a)   **(b)**

Fig. 7   **Array system (a) and blade chord and twist radial distributions (b) (adapted from Ref. [25]).**

Table 2   Parameters for the array of propellers case

Parameter	Value	Unit
Flight altitude - h	0	m
Freestream velocity - V_f	30.23	$m\,s^{-1}$
Propeller diameter - D	0.2032	m
Hub-to-tip ratio - r_{hub}/r_{tip}	0.1095	-
Number of blades - N_B	6	-
Blade pitch at $r/R = 0.07$	30	°
Rotational speed - RPS	148.8	rps
Tip clearance - d/D	0.02	-
Relative blade-phase angle - $\Delta\phi$	0	°

As previously mentioned, the low-fidelity tool used aerodynamic data from high-fidelity simulations to determine the flow field. Due to the small tip clearance between propellers, aerodynamic interaction affects the load distribution over the blades. Fig. 8a shows the loading distribution of the middle propeller, whereas Fig. 8b compares the thrust distribution difference at the propeller disk plane to an isolated case (with no aerodynamic interference). As the blades of the middle propeller approach those of the adjacent propellers, the thrust reduces until it reaches the horizontal plane (along the y-axis). Then, the thrust increases during the retreat. The most significant variations occur near the blade tip and close to the y-axis but are present throughout most of the propeller disk.
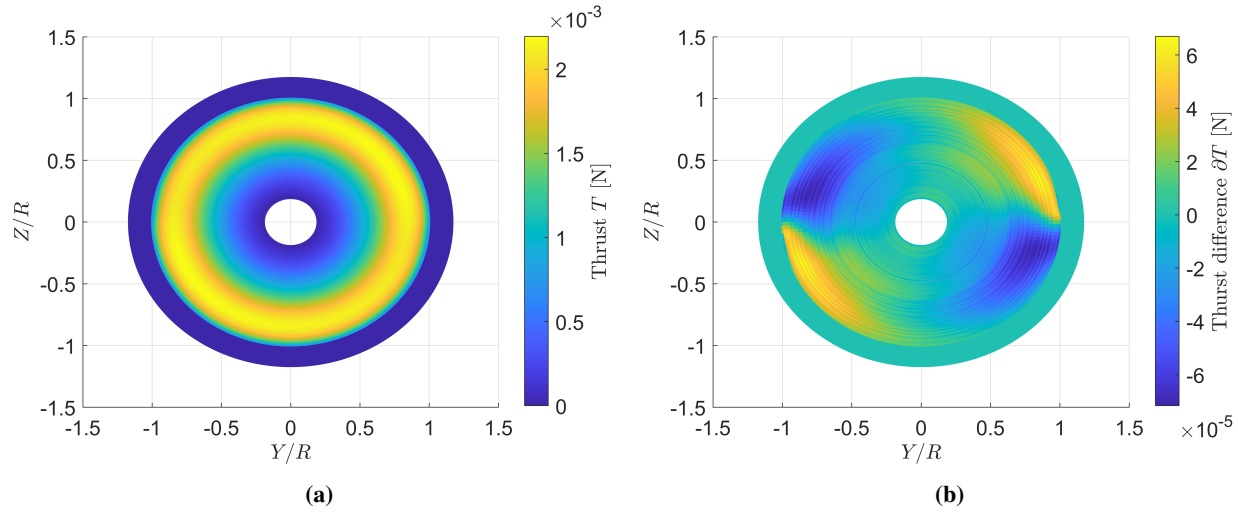

Fig. 8   Middle propeller load data: (a) thrust distribution and (b) thrust distribution difference due to aerodynamic interaction.

The blade was discretized using a grid of 50 chordwise points and 100 radial points, providing enough refinement to capture the loading differences near the blade tip. The time was discretized with an initial estimate of 400 steps per period. Acoustic pressures were computed at six microphone positions: three in the xy-plane (Fig. 9a) and three in the xz-plane (Fig. 9b). All microphones are located at a distance of $10D$ from the center of the middle propeller.
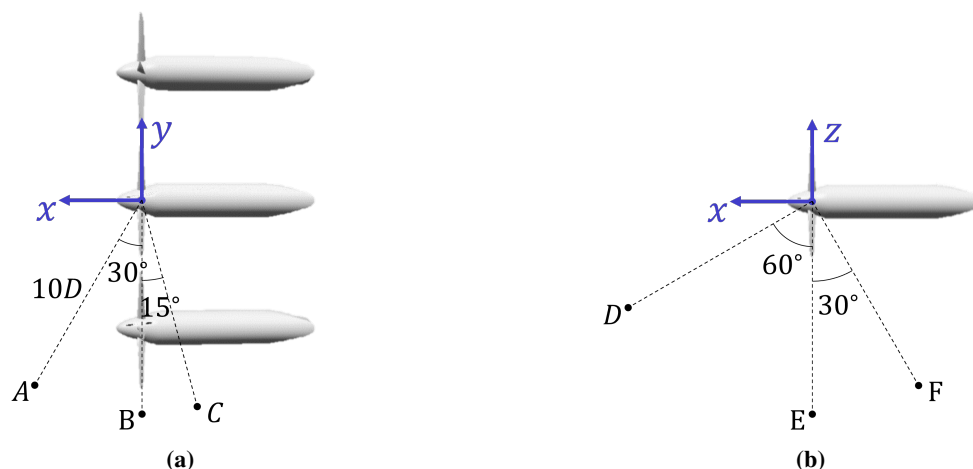
9

Fig. 9 Microphones positions in the (a) xy-plane, and (b) in the xz-plane (adapted from Ref. [25]).

Fig. 10 shows the overall sound pressure level (OSPL) computed values at various azimuthal locations obtained from high-fidelity simulations (indicated by HF) and the low-fidelity tool (indicated by LF). The best agreement is at the plane disk (points B and E) and gets progressively worse as the location moves away from this plane. This is expected because, as the observer moves in the direction of the propeller axis, the broadband noise becomes more dominant. Thus, the most significant difference occurs at point D, with a difference of about 3.6 dB, while the differences at points B and E are as low as 0.6 dB. The results trend is similar to that seen in the isolated propeller case. Nevertheless, the comparison indicates that the low-fidelity tool can adequately predict the noise emitted by a distributed propeller system at different azimuthal positions, with better results as the observer location approaches the plane of the propeller disk.
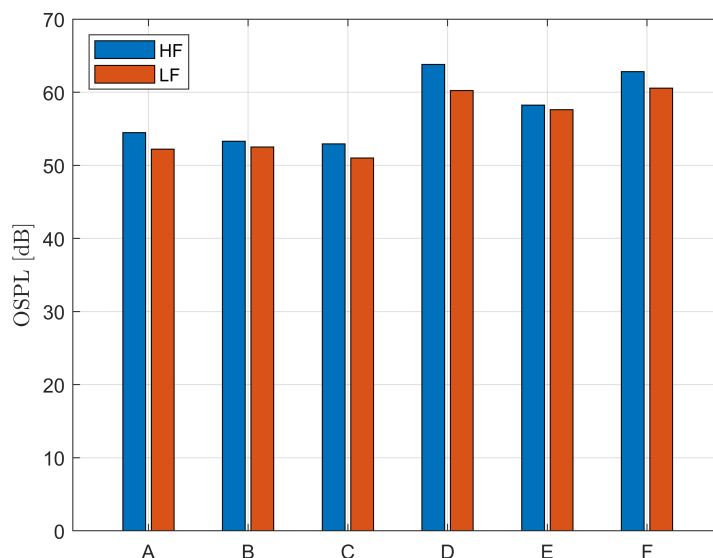

Fig. 10 Comparison of the OSPL computed with high-fidelity simulations (HF) and the low-fidelity tool (LF).

V. Tool Application Example

This section provides an example of how the low-order acoustic prediction tool can be used to estimate the impact of aerodynamic interference on the noise emitted by DP configurations. For this analysis, the same propeller and data

presented in Sec. IV.B was used. The example shows a noise directivity study of the propeller operating in a uniform flow (no aerodynamic interference) and in the same operating conditions but under a flow field disturbed by adjacent propellers (using the unsteady blade loading presented in Fig. 8a). By comparing the results, the low-order numerical tool reveals the acoustic relevance of aerodynamic interference in configurations where the propellers are close enough to affect the flow field of neighboring propellers.

Figure 11 displays the analysis of the source directivity at the first BPF in the xy-plane. The sound pressure level (SPL) values are shown for the steady case (indicated by ISO) and the unsteady case (indicated by DP). The aerodynamic inputs for both were obtained from high-fidelity simulations, as described in Sec. IV. The unsteady blade loading used in the DP case is the same as that presented in Fig. 8a, which pertains to the middle propeller shown in Fig. 7a.
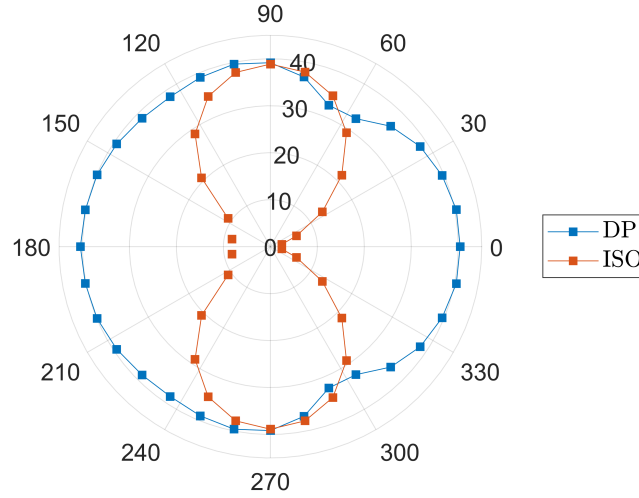

Fig. 11 Comparison of the first BPF values between the isolated propeller (ISO) and the middle propeller of the array configuration (DP) at xy-plane.

Upon initial inspection, it is evident that the two cases display contrasting behaviors. In the case where an isolated propeller operates in a uniform flow (ISO), the maximum sound pressure level (SPL) occurs at the rotor plane and decreases as it moves closer to the propeller axis. In contrast, the maximum SPL in the DP case occurs at the propeller axis and decreases as it approaches the rotor plane. This same trend was also observed in the study by Koutsoukos [25]. At the rotor plane, the SPL difference between the cases with and without aerodynamic interference is only around 0.5 dB. However, as the emission angle approaches the propeller axis, the SPL at the first BPF of the DP case surpasses 40 dB, which is a significant increase compared to the isolated propeller. Since the only distinction between both computations is the aerodynamic input, it is clear that the observed differences are caused by the discrepancies in blade loading due to interferences between the adjacent propellers. Therefore, near the propeller axis, the disparity between both cases is not only due to a lack of a broadband model in the code, but also to aerodynamic interference.

To put it succinctly, the acoustic tool can provide an efficient way to estimate and compare noise emissions from distributed propeller configurations. It is particularly useful for investigating the impact of aerodynamic interference on the acoustic footprint, as demonstrated above. By using this tool, users can make informed decisions about the noise impact of various DP systems, helping mitigate noise pollution and ensure regulatory compliance for new aircraft configurations.

VI. Conclusions and future work

This paper presented a tool for predicting the tonal noise radiated by a distributed propeller system. The computation requires geometric input data related to the DP system, propeller, and blade, observer position, and system operating conditions. The low-numerical tool was tested against high-fidelity simulations for an isolated propeller. For the isolated propeller, the difference between both approaches was less than 6 dB at the azimuthal position of 30°, and decreased to 0.15 dB at 90°. The large discrepancy in noise predictions near the propeller axis is a result of the broadband noise dominating this area, which the low-order tool is not designed to capture. Instead, the tool primarily focuses

on predicting the tonal component of the noise. Yet, these results indicate that it can accurately compute tonal noise emissions from an isolated propeller, even when it uses aerodynamic input data obtained from a BEMT model.

It has also demonstrated its ability to predict the noise of multiple propellers under aerodynamic interaction. In this case, the aerodynamic input was obtained from high-fidelity simulations as described in Sec. IV. It predicted adequately at different azimuthal positions, with better results as the observer came closer to the rotor plane (about 0.6 dB). Thus, the approach presented offers a practical advantage by allowing for a fast analysis of the combined effect of aerodynamic and acoustic interference on the noise emissions of a distributed propeller system.

While the tool may not produce results as precise as high-fidelity simulations in areas where broadband noise dominates, it still provides a valuable estimation of noise emissions and can be utilized for comparing the tonal noise of various configurations. The tool is particularly useful for investigating the impact of aerodynamic interference on the acoustic footprint of DP systems, as demonstrated in the example provided in the previous section. By using it, users can make informed decisions about the noise impact of various DP systems, helping mitigate noise pollution and ensure regulatory compliance for new aircraft configurations.

Overall, the approach presented here has the potential to contribute to studies regarding configurations where propellers are under significant aerodynamic interference. With it validated, a more detailed investigation of such effects in synchrophasing cases will be pursued in future work. Further work will also focus on adding a broadband model and exploring its potential for analyzing noise emissions from other types of propulsive configurations with multiple propellers.

Acknowledgments

References

[1] Pyrzyk, A. E., "Flightpath 2050 - Europe's Vision for Aviation," Tech. rep., 2014. https://doi.org/10.2777/50266.

[2] Kim, H. D., "Distributed Propulsion Vehicles," *27th International Congress of the Aeronautical Sciences*, Vol. 1, 2010, pp. 1–11.

[3] Stoll, A. M., Bevirt, J. B., Moore, M. D., Fredericks, W. J., and Borer, N. K., "Drag Reduction Through Distributed Electric Propulsion," *14th AIAA Aviation Technology, Integration, and Operations Conference*, Atlanta, GA, 2014, pp. 1–10. https://doi.org/10.2514/6.2014-2851.

[4] Deere, K. A., Viken, S., Carter, M., Viken, J. K., Derlaga, J. M., and Stoll, A. M., "Comparison of High-Fidelity Computational Tools for Wing Design of a Distributed Electric Propulsion Aircraft," *35th AIAA Applied Aerodynamics Conference*, 2017, pp. 1–22. https://doi.org/10.2514/6.2017-3925.

[5] Herzog, N., Reeh, A., Kümmel, A., and Breitsamter, C., "Analysis of Distributed Electric Propulsion on Commuter Aircraft," *AIAA Scitech 2021 Forum*, 2021, pp. 1–16. https://doi.org/10.2514/6.2021-1199.

[6] Pascioni, K. A., and Rizzi, S. A., "Tonal Noise Prediction of a Distributed Propulsion Unmanned Aerial Vehicle," *2018 AIAA/CEAS Aeroacoustics Conference*, 2018, pp. 1–18. https://doi.org/10.2514/6.2018-2951.

[7] Pascioni, K. A., Rizzi, S. A., and Schiller, N. H., "Noise Reduction Potential of Phase Control for Distributed Propulsion Vehicles," *AIAA Scitech 2019 Forum*, 2019, pp. 1–16. https://doi.org/10.2514/6.2019-1069.

[8] Patterson, A., Schiller, N. H., Ackerman, K. A., Gahlawat, A., Gregory, I. M., and Hovakimyan, N., "Controller Design for Propeller Phase Synchronization With Aeroacoustic Performance Metrics," *AIAA Scitech 2020 Forum*, 2020. https://doi.org/10.2514/6.2020-1494.

[9] Johnston, J. F., Donham, R. E., and Guinn, W. A., "Propeller Signatures and Their Use," *Journal of Aircraft*, Vol. 18, No. 11, 1981, pp. 934–942. https://doi.org/10.2514/6.1980-1035.

[10] Magliozzi, B., "Synchrophasing for Cabin Noise Reduction of Propeller-Driven Airplanes," *AIAA 8th Aeroacoustics Conference*, 1983, pp. 1–8. https://doi.org/10.2514/6.1983-717.

[11] Fuller, C. R., "Noise Control Characteristics of Synchrophasing. I - Analytical Investigation," *AIAA Journal*, Vol. 24, No. 7, 1986, pp. 1063–1069. https://doi.org/10.2514/6.1984-2369.

[12] Jones, J. D., and Fuller, C. R., "Noise Control Characteristics of Synchrophasing. II - Experimental Investigation," *AIAA Journal*, Vol. 24, No. 8, 1986, pp. 1271–1276. https://doi.org/10.2514/3.9431.

[13] Chirico, G., Barakos, G. N., and Bown, N., "Propeller Installation Effects on Turboprop Aircraft Acoustics," *Journal of Sound and Vibration*, Vol. 424, 2018, pp. 238–262. https://doi.org/10.1016/j.jsv.2018.03.003.

[14] Bernardini, G., Centracchio, F., Iemma, U., Pasquali, C., Poggi, C., Rossetti, M., and Serafini, J., "Aeroacoustic Numerical Characterization of Propellers Interaction," *26th International Congress on Sound and Vibration*, 2019, pp. 1–8.

[15] Bernardini, G., Centracchio, F., Gennaretti, M., Iemma, U., Pasquali, C., Poggi, C., Rossetti, M., and Serafini, J., "Numerical Characterisation of the Aeroacoustic Signature of Propeller Arrays for Distributed Electric Propulsion," *Applied Sciences*, Vol. 10, No. 8, 2020, pp. 1–18. https://doi.org/10.3390/APP10082643.

[16] de Vries, R., van Arnhem, N., Sinnige, T., Vos, R., and Veldhuis, L. L., "Aerodynamic Interaction Between Propellers of a Distributed-Propulsion System in Forward Flight," *Aerospace Science and Technology*, Vol. 118, 2021, pp. 1–20. https://doi.org/10.1016/j.ast.2021.107009.

[17] Poggi, C., Bernardini, G., and Gennaretti, M., "Aeroacoustic Analysis of Wing-Mounted Propeller Arrays," *AIAA Aviation 2021 Forum*, 2021, pp. 1–13. https://doi.org/10.2514/6.2021-2236.

[18] de Vries, R., van Arnhem, N., Avallone, F., Ragni, D., Vos, R., Eitelberg, G., and Veldhuis, L. L. M., "Experimental Investigation of Over-the-Wing Propeller–Boundary-Layer Interaction," *AIAA Journal*, Vol. 59, No. 6, 2021, pp. 2169–2182. https://doi.org/10.2514/1.j059770.

[19] Hanson, D., "Near Field Noise of High Tip Speed Propellers in Forward Flight," *3rd AIAA Aeroacoustics Conference*, 1976, pp. 1–13. https://doi.org/10.2514/6.1976-565.

[20] Ffowcs-Williams, J. E., and Hawkings, D. L., "Sound Generation by Turbulence and Surfaces in Arbitrary Motion," *Philosophical Transactions of the Royal Society of London. Series A, Mathematical and Physical Sciences*, Vol. 264, No. 1151, 1969, pp. 321–342. https://doi.org/10.1098/rsta.1969.0031.

[21] Hanson, D. B., "Propeller Noise Caused by Blade Tip Radial Forces," *AAIA 10th Aeroacosutics Conference*, 1986, pp. 1–10. https://doi.org/10.2514/6.1986-1892.

[22] Wells, V. L., "Analysis of the Acoustic Planform Method for Rotor Noise Prediction," *AIAA Journal*, Vol. 26, No. 5, 1988, pp. 522–523. https://doi.org/10.2514/3.9928.

[23] Brentner, K. S., and Farassat, F., "Modeling Aerodynamically Generated Sound of Helicopter Rotors," *Progress in Aerospace Sciences*, Vol. 39, No. 2-3, 2003, pp. 83–120. https://doi.org/10.1016/S0376-0421(02)00068-4.

[24] Fuerkaiti, Y., Grande, E., Casalino, D., Avallone, F., and Ragni, D., "Efficient Low-Fidelity Aeroacoustic Permanence Calculation of Propellers," *Aerospace Science and Technology*, Vol. 123, No. 107438, 2022, pp. 1–11. https://doi.org/10.1016/j.ast.2022.107438.

[25] Koutsoukos, A., *Aerodynamic and Aeroacoustic Interaction Effects of a Distributed-Propeller Configuration in Forward Flight*, Delft, 2022. URL http://resolver.tudelft.nl/uuid:b746cbbe-2fc0-4506-a82a-b320e476521a.

[26] Hanson, D. B., "Helicoidal Surface Theory for Harmonic Noise of Propellers in the Far Field," *AIAA Journal*, Vol. 18, No. 10, 1980, pp. 1213–1220. https://doi.org/10.2514/3.50873.

[27] van Arnhem, N., de Vries, R., Sinnige, T., Vos, R., Eitelberg, G., and Veldhuis, L. L., "Engineering Method to Estimate the Blade Loading of Propellers in Nonuniform Flow," *AIAA Journal*, Vol. 58, No. 12, 2020, pp. 5332–5346. https://doi.org/10.2514/1.J059485.